Journal of Multidisciplinary Healthcare

Dovepress
open access to scientific and medical research

Open Access Full Text Article

ORIGINAL RESEARCH

Validation and Feasibility of Ultrafast Cervical Spine MRI Using a Deep Learning-Assisted 3D Iterative Image Enhancement System

Hui Yao, Bangsheng Jia, Xuelin Pan, Jiayu Sun

Department of Radiology, West China Hospital of Sichuan University, Chengdu, 610041, People's Republic of China

Correspondence: Jiayu Sun, Department of Radiology, West China Hospital of Sichuan University, Guoxue Xiang No. 37, Chengdu, Sichuan, 610041, People's Republic of China, Email sunjiayu20232023@163.com

Purpose: This study aimed to evaluate the feasibility of ultrafast (2 min) cervical spine MRI protocol using a deep learning-assisted 3D iterative image enhancement (DL-3DIIE) system, compared to a conventional MRI protocol (6 min 14s).

Patients and Methods: Fifty-one patients were recruited and underwent cervical spine MRI using conventional and ultrafast protocols. A DL-3DIIE system was applied to the ultrafast protocol to compensate for the spatial resolution and signal-to-noise ratio (SNR) of images. Two radiologists independently assessed and graded the quality of images from the dimensions of artifacts, boundary sharpness, visibility of lesions and overall image quality. We recorded the presence or absence of different pathologies. Moreover, we examined the interchangeability of the two protocols by computing the 95% confidence interval of the individual equivalence index, and also evaluated the inter-protocol intra-observer agreement using Cohen's weighted kappa.

Results: Ultrafast-DL-3DIIE images were significantly better than conventional ones for artifacts and equivalent for other qualitative features. The number of cases with different kinds of pathologies was indistinguishable based on the MR images from ultrafast-DL -3DIIE and conventional protocols. With the exception of disc degeneration, the 95% confidence interval for the individual equivalence index across all variables did not surpass 5%, suggesting that the two protocols are interchangeable. The kappa values of these evaluations by the two radiologists ranged from 0.65 to 0.88, indicating good-to-excellent agreement.

Conclusion: The DL-3DIIE system enables 67% spine MRI scan time reduction while obtaining at least equivalent image quality and diagnostic results compared to the conventional protocol, suggesting its potential for clinical utility.

Keywords: cervical spine, magnetic resonance imaging, fast imaging, deep learning

Introduction

Magnetic Resonance Imaging (MRI) of the cervical spine non-invasively delivers high-resolution visuals, capturing subtle changes in both the spinal cord and surrounding tissues.[1,2] It excels in delineating soft tissues such as the spinal cord, nerves, and intervertebral discs.[1] However, it confronts an inherent trade-off: prolonged acquisition time compromises either spatial resolution or signal-to-noise ratio (SNR), thereby limiting its clinical utility. Time-consuming spine MRI increases the likelihood of patient movement, introducing artifacts or blurring into images.[3] Moreover, extended MRI exams pose challenges for patients, especially those experiencing claustrophobia or difficulties in remaining still. Unfortunately, as the primary participants for spinal MRI, seniors or patients with severe spinal disease are more likely to be distressed about staying still for long periods, which further raises the opportunity of motion artifacts during exams.

In the past three decades, various acceleration techniques have been introduced in MRI.[4–7] Parallel imaging harnesses multiple receiver coils to simultaneously collect the MRI data.[8] Partial Fourier capitalizes on inherent data redundancy due to Hermitian symmetry, collecting only a fraction of the k-space.[9] Compressed sensing undersamples the k-space leveraging sparsity of images.[10] Nowadays, by integrating these acceleration techniques, routine spine MRI has already trimmed its total acquisition time to approximately 5 minutes without compromising diagnostic performance.[5] However,

Received: 20 February 2024
Accepted: 13 May 2024
Published: 22 May 2024

the footsteps towards faster skeletal imaging should not be ended. Despite the achievement, spine MRI still holds much longer acquisition time compared to CT.

Recently, deep learning (DL) assisted image optimization has brought fresh possibilities in medical imaging, especially for MRI.[11] The critical idea of DL approaches is to exploit the empirical information of structures and patterns from previously acquired images. In addition to image quality improvement, a common strategy is to speed up sequences with fewer acquisitions while recovering quality to clinically acceptable standards, using this empirical information.[11] Different technical branches have been established, including DL-based reconstruction and post-processing. The former is currently popular, including algorithms provided by several MR vendors.[12–15] However, reconstruction relies on the utilization of raw k-space data. Therefore, retrospective use of previous images is almost impossible. Also, it is hard to imagine inter-vendor universality for these approaches due to commercial reasons. In contrast, DL-based post-processing approaches are free from these drawbacks. Denoising techniques excel in estimating noise from true signal.[16] Image sharpening estimates the boundaries of anatomy or lesions, quite useful in spine MRI where tiny structures and air-filler cavities exist.[17] DL super-resolution, compared to zero-filling or bi-spline interpolations, performs better by training from the low- and high-resolution MRI dictionaries.[18] Applications of these raw-data-free methods in musculoskeletal MRI are emerging.[19] Importantly, these image enhancement approaches are independent of the existing acceleration techniques like parallel imaging and compressed sensing, and could in principle integrate with them.[20] Strategies of ultrafast acquisition for spine imaging under 2 minutes, with the cooperation of DL reconstruction, have already emerged.[20,21] However, research on ultrafast skeletal MRI strategies using post-processing DL methods is still rare to our knowledge.

In this study, we proposed a set of ultrafast cervical spine MRI protocols utilizing a deep learning-assisted 3D iterative image enhancement (DL-3DIIE) system to achieve a total acquisition time of 2 min. To explore whether these protocols reserve the feasibility for diagnosis in outpatient physical examination, we compared them with the conventional protocol set accelerated by parallel imaging, which is in routine usage of clinical practice.

Materials and Methods

Participants

The prospective study was approved by the local ethics committee of West China Hospital and written informed consent was obtained for all patients. All procedures performed in studies involving human participants were in accordance with the 1975 Declaration of Helsinki, as revised in 2013. Sixty participants who felt discomfort in the spine or surrounding muscles were consecutively recruited from the physical examination center of our hospital for spine MRI examination between September 2022 and July 2023. Participants were excluded if: 1) no complete cervical spine MRI scan; 2) the presence of metallic hardware and excessive motion artifacts seen on MRI scans rendering images non-diagnostic. Finally, 51 patients were included in our study. For each participant, we collected a range of data that included demographic and clinical information, patient history, and MRI data.

Image Acquisition

Cervical spine MRI examinations were conducted using a 1.5 T MRI scanner (Avanto, Siemens Healthineers, Erlangen, Germany) equipped with a 32-element phased-array surface spine coil. All patients underwent conventional and ultrafast protocols, and both protocols included three sequences: sagittal T1-weighted (T1WI) and T2-weighted (T2WI), and axial T2-weighted images. The overall strategy of our ultrafast protocols is (1) reduce the number of averages to shorten the acquisition time at the cost of reduced SNR; (2) reduce the in-plane resolution to increase the SNR as well as shorten acquisition time; (3) compensate for the reduced SNR and blurred edges by applying patch-based iterative denoising and machine-learning super-resolution; (4) All other parameters, including thickness and parallel imaging accelerating factor, were kept still if possible. As a result, the total acquisition time of the ultrafast protocol was reduced to 2 min, while that of the conventional protocol was 6 min 14s. The detailed MRI protocols are presented in Table 1.

Table 1 Acquisition Parameters and Scan Times for Conventional and Ultrafast Protocols

Sequence	Conventional	Ultrafast	Conventional	Ultrafast	Conventional	Ultrafast
	Sagittal T1WI (TSE)		Sagittal T2WI FS (TSE-FS)		Axial T2WI (GRE-FS)	
TR/TE (ms)	440/11	440/11	2700/78	2700/78	447/21	383/18
Flip angle (°)	150	150	150	150	30	30
Field of view (mm)	240 x 240	240 x 240	240 x 240	240 x 240	180 x 180	180 x 180
Matrix size	384 x 268	256 x 180	384 x 308	256 x 205	384 x 308	256 x 205
Slice thickness (mm)	3.0	3.0	3.0	3.0	3.0	3.0
Echo train length	3	3	18	18	1	1
Number of averages	4	2	2	1	2	1
Acceleration factor	2	2	2	2	2	2
Scan time (min:s)	2:22	0:47	1:24	0:27	2:28	0:46
Total scan time (min:s)	Conventional: 6:14			Ultrafast: 2:00		

Abbreviations: FS, fat suppression; GRE, gradient recalled echo; TE, echo time; TR, repetition time; TSE, turbo spin echo; WI, weighted image.

Deep Learning-Based Image Enhancement

The DL-3DIIE system works on an external workstation (iQMR, Medic Vision Imaging Solutions, Tirat Carmel, Israel) which is FDA-approved. It includes only post-processing procedures, without k-space data involved. The original MR images from the scanner are transmitted to the workstation for the following procedures:

(1) Initialization: The images first underwent an inverse-Fourier transformation. An initial denoising was performed using a k-space filter, aimed to improve the stability of the further steps.[22]
(2) DL Super-Resolution: A zero-filling by 1.75 was performed to obtain pseudo high-resolution images. After that, a pre-trained deep learning model using convolutional neural networks (CNN)-based filtering was utilized for the super-resolution. It was trained using more than 30,000 multi-vendor MRI sequences including 400,000 2D human images. The input data for training was low-resolution images down-sampled by a designed k-space filter, while the ground truth for training was the unfiltered high-resolution images.

(3) Iterative Enhancement: This step takes advantage of the self-similarity of the image. A 3D patch decomposition was applied with both the patch features and noise estimation updated in each iteration, similar to other classic patch-based self-similarity learning approaches.[23] This image enhancement method was developed from the non-local means method,[24] and was previously applied in brain MRI and low-dose CT studies.[25,26]
(4) Convergence: Ideally, the separated real MR image should be smooth, while the noise map should follow Gaussian distribution or at least with degraded structural details.[24,27] Therefore, convergence criteria including patch similarity and noise variation were applied.

In summary, the DL-3DIIE system incorporates both a conventional patch-based method and a deep learning method. The whole procedure took approximately 20 seconds for each MR sequence. All the images are stored and analyzed in DICOM format.

Image Quality Assessment

The human eye is the golden standard for medical imaging quality. A bi-reader randomized, blinded assessment was taken to compare image quality. Two radiologists (HY and BJ with 8 and 6 years of experience in musculoskeletal radiology, respectively) independently reviewed all the images. The example of sagittal T1WI and T2WI, and axial T2WI obtained from conventional, ultrafast and ultrafast-DL-3DIIE protocols are shown in Figure 1. The conventional and ultrafast-DL-3DIIE images were evaluated separately and the order of cases in each evaluation was randomized. The observers, who were blinded to the clinical information and protocol type, assessed and graded the quality of images from the dimensions of artifacts, boundary sharpness,

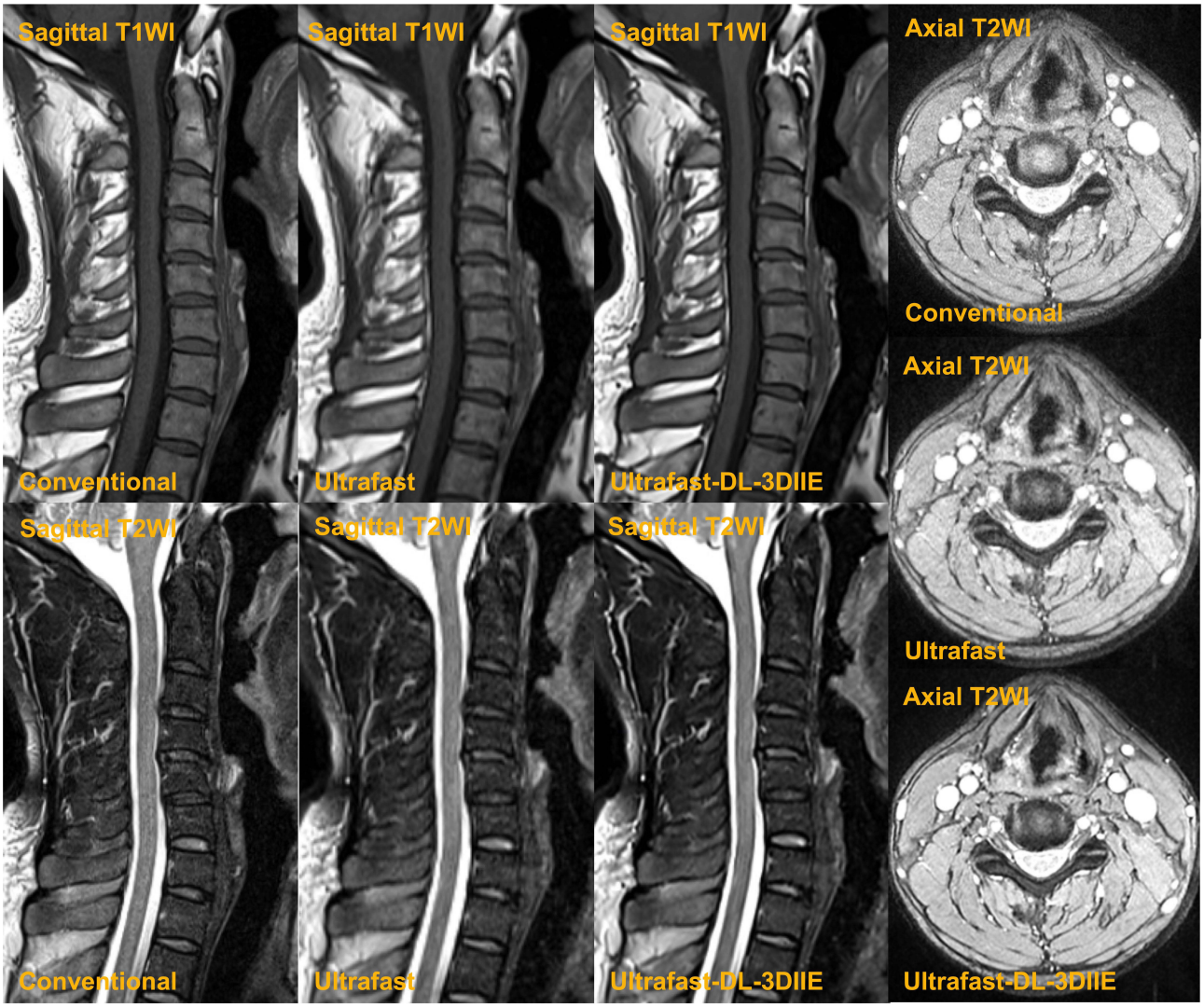

Figure 1 The example of sagittal T1-weighted (T1WI) and T2-weighted (T2WI), and axial T2-weighted images, obtained from conventional, ultrafast and ultrafast-DL-3DIIE protocols.

visibility of lesions and overall image quality, using a 5-point Likert scale (range: 1 = "worst" to 5 = "best"). Moreover, the SNRs of different regions, cord/cerebrospinal fluid (CSF) contrast and structural similarity index (SSIM) were calculated by each observer. Four circular regions of interest (ROIs) with a diameter of 3 mm were located in the spinal cord, CSF, vertebral body and intervertebral discs, respectively. The SSIM calculation was employed to assess for absolute errors (anatomic or pathologic data loss or aberration).

Diagnostic Assessment

After judging the image quality, the diagnostic assessment was carried out at the individual level. Based on strategies from previous studies.[28–35] the radiologists independently recorded the presence or absence of pathologies of each participant, including central canal stenosis, foraminal stenosis, endplate degeneration, disc degeneration, and disc herniation. At this step, images of all three sequences (sagittal T1WI and T2WI, and axial T2WI) could be viewed by the radiologists. After assessing all the cases, the radiologists would discuss the cases with distinct records, and finally reach a consensus.

Statistical Analysis

The interchangeability of the two protocols was confirmed to assess whether a new imaging protocol can replace an existing one by ensuring that the agreement rate, when one observer uses the new technique, is not significantly lower than when both observers use the existing technique.[36,37] We calculated the intra-protocol inter-observer agreement rate (both observers assessed the conventional protocol images) and the inter-protocol inter-observer agreement rate (one observer evaluated the conventional protocol images, while the other observer evaluated the ultrafast protocol images) for each variable. The individual equivalence index was obtained by subtracting the inter-protocol inter-observer agreement rate from the intra-protocol inter-observer agreement rate. Furthermore, we computed the 95% confidence interval (95% CI) using bootstrapping methods with 1000 repetitions. The interchangeability of the two protocols was established when the 95% CI of the individual equivalence index was less than 5%.

Cohen's weighted kappa was used to evaluate inter-protocol intra-observer agreements of the two observers for all variables from the three cervical spine MRI sequences. We also assessed the intra-protocol inter-reader agreement (both readers evaluated the conventional protocol images) and inter-protocol inter-reader agreement. The kappa value was interpreted as follows: less than 0.20, poor agreement; 0.21–0.40, fair agreement; 0.41–0.60, moderate agreement; 0.61–0.80, good agreement; and 0.81–1.00, excellent agreement. Additionally, two-tailed *t*-tests or chi-squared tests were performed to assess the statistical significance of the differences for all variables from the ultrafast and conventional protocols. Power analysis was conducted using the scripts of sampsizepwr in Matlab (MathWorks, Natick, Massachusetts, USA) to calculate the power for the sample size in this study. All the statistical analyses were performed using MATLAB (MathWorks, Natick, Massachusetts, USA). The threshold for statistical significance was set at $p < 0.05$, using Bonferroni correction for multiple comparisons.

Results

Participant Characteristics

After enrollment and exclusion, we finally included 51 participants (31 men and 20 women; age, 51.7 ± 12.5 years; age range, 30–80 years) in this study. Among the cohort, 49 (96.1%) were diagnosed as single or multiple pathologies in the cervical spine, after the integration of image evaluation results by the two radiologists. The counts of each pathology were: central canal stenosis (9, 17.6%), foraminal stenosis (8, 15.7%), endplate degeneration (4, 7.8%), disc degeneration (47, 92.2%), disc herniation (45, 88.2%) and other pathologies (17, 33.3%).

Comparison of Qualitative Assessment

Artifacts were significantly reduced in ultrafast-DL-3DIIE images (including sagittal T1WI and T2WI, and axial T2WI) compared with conventional ones ($p = 0.021$, after Bonferroni correction). Boundary sharpness, visibility of lesions and overall image quality were not significantly different between the three kinds of images from the two protocols (all p values > 0.1, after Bonferroni correction). Inter-observer agreements (Cohen's weighted kappa) between the two observers in the artifacts, boundary sharpness, visibility of lesions and overall image quality were all good: 0.65, 0.77, 0.72, and 0.73, respectively (Table 2).

Comparison of Quantitative Assessment

The assessment results of SNRs and cord/CSF contrast noise ratio (CNR) are shown in Table 3. They all showed significant improvement for ultrafast-DL-3DIIE images, compared to the corresponding ultrafast and conventional ones (all p values > 0.05, after Bonferroni correction). Based on current sample size of 51 participants, the powers of the significant group differences for both qualitative and quantitative assessment were all larger than 0.80. Moreover, the quantitative assessment of image similarity using the SSIM was 0.95 ± 0.06 for ultrafast vs ultrafast-DL-3DIIE, which supported the absence of substantial anatomic aberration by deep learning processing of the source images.

Table 2 Qualitative Assessment and Comparison

	Score (1–5)			P-value	Inter-Observer Agreement
	Conventional	Ultrafast-DL-3DIIE	Ultrafast	Conventional vs Ultrafast-DL-3DIIE	
Avoidance of Artifacts	2.8 ± 0.6	3.2 ± 0.8	3.0 ± 0.7	0.021*	0.68 (0.62–0.74)
Boundary sharpness	3.8 ± 0.9	3.5 ± 0.7	2.5 ± 0.6	0.12	0.77 (0.73–0.81)
Visibility of lesions	3.8 ± 0.8	3.6 ± 0.7	2.8 ± 0.5	0.44	0.72 (0.69–0.75)
Overall image quality	3.5 ± 0.8	3.4 ± 0.6	2.5 ± 0.5	> 0.90	0.73 (0.68–0.78)

Notes: Cohen's weighted kappa values (95% confidence interval) for inter-observer agreement are shown. The p values were calculated with two-tailed *t*-tests, after Bonferroni correction for multiple comparisons. The symbol (*) indicates being significant.
Abbreviation: DL-3DIIE, deep learning-assisted 3D iterative image enhancement.

Table 3 Quantitative Assessment and Comparison

	Measurement			P-value
	Conventional	Ultrafast-DL-3DIIE	Ultrafast	Conventional vs Ultrafast-DL-3DIIE
Sagittal T1-weighted image				
SNR (spinal cord)	61.2 ± 21.3	115.4 ± 40.5	58.2 ± 20.1	< 0.001
SNR (CSF)	29.9 ± 9.8	53.4 ± 16.5	32.4 ± 9.3	< 0.001
SNR (vertebrae)	107.3 ± 36.7	200.4 ± 68.7	101.5 ± 39.2	< 0.001
SNR (disc)	61.9 ± 17.3	118.8 ± 39.4	63.2 ± 18.1	< 0.001
Cord/CSF CNR	31.3 ± 8.7	62.0 ± 25.1	25.8 ± 9.4	< 0.001
Sagittal T2-weighted image				
SNR (spinal cord)	70.3 ± 25.8	164.6 ± 65.5	73.1 ± 22.4	< 0.001
SNR (CSF)	160.7 ± 56.4	405.4 ± 143.8	152.7 ± 50.5	< 0.001
SNR (vertebrae)	37.8 ± 12.9	91.5 ± 38.7	35.2 ± 11.9	< 0.001
SNR (disc)	41.2 ± 13.4	105.1 ± 39.5	39.1 ± 12.4	< 0.001
Cord/CSF CNR	90.4 ± 31.2	240.8 ± 88.3	89.6 ± 33.2	< 0.001
Axial T2-weighted image				
SNR (spinal cord)	84.1 ± 31.8	174.2 ± 61.0	82.2 ± 30.1	< 0.001
SNR (CSF)	125.2 ± 46.9	259.3 ± 78.2	132.4 ± 39.3	< 0.001
SNR (vertebrae)	30.5 ± 11.4	57.1 ± 19.8	29.3 ± 9.2	< 0.001
SNR (disc)	71.8 ± 21.5	156.2 ± 49.5	63.2 ± 18.1	< 0.001
Cord/CSF CNR	41.1 ± 15.7	85.1 ± 28.5	50.2 ± 17.7	< 0.001

Note: The p values were calculated with two-tailed *t*-tests, after Bonferroni correction for multiple comparisons.
Abbreviations: CNR, contrast noise ratio; CSF, cerebrospinal fluid; DL-3DIIE, deep learning-assisted 3D iterative image enhancement; SNR, signal-to-noise ratio.

Diagnostic Performance

The number of cases with different pathologies reported by the two observers is presented in Table 4. The pathologies included central canal stenosis (representative case: Figure 2a and b), foraminal stenosis (representative case: Figure 2c and d), endplate degeneration, disc degeneration (representative case: Figure 3a and b), disc herniation (representative case: Figure 3c and d) and others (hyperintense cord lesion, retro-odontoid pseudotumor, spinal lipoma, vertebral fracture and vertebral hypointense lesion). The diagnostic results were significantly indistinguishable based on the MR images from ultrafast-DL-3DIIE and conventional protocols (all p values > 0.05, after Bonferroni correction). Table 4 also shows the kappa values for the inter-protocol intra-observer agreement, intra-protocol (conventional vs conventional) inter-observer agreement, and inter-protocol inter-observer agreement. The inter-protocol intra-observer agreement (kappa

Table 4 Integrated Results of Diagnostic Performance by Two Observers

	Count of Cases (With/Without)		P-value Conventional vs Ultrafast-DL-3DIIE	Inter-Protocol Intra-Observer Agreement	Intra-Protocol Inter-Observer Agreement	Inter-Protocol Inter-Observer Agreement
	Conventional	Ultrafast-DL-3DIIE				
Central canal stenosis	9/42	10/41	> 0.90	0.85 (0.81–0.89)	0.73 (0.69–0.77)	0.72 (0.68–0.76)
Foraminal stenosis	8/43	9/42	> 0.90	0.87 (0.85–0.89)	0.75 (0.72–0.78)	0.73 (0.70–0.76)
Endplate degeneration	4/47	8/43	0.36	0.67 (0.61–0.73)	0.54 (0.49–0.59)	0.51 (0.47–0.55)
Disc degeneration	47/4	41/10	0.15	0.65 (0.60–0.70)	0.51 (0.44–0.58)	0.50 (0.45–0.55)
Disc herniation	45/6	43/8	0.77	0.88 (0.85–0.91)	0.78 (0.74–0.82)	0.75 (0.72–0.78)
Other pathologies	17/34	14/37	0.67	0.82 (0.78–0.86)	0.68 (0.63–0.73)	0.66 (0.63–0.69)

Notes: Other pathologies included hyperintense cord lesion, retro-odontoid pseudotumor, spinal lipoma, vertebral fracture and vertebral hypointense lesion. Cohen's weighted kappa values (95% confidence interval) for agreement evaluation are shown. The p values were calculated with chi-squared tests.
Abbreviation: DL-3DIIE, deep learning-assisted 3D iterative image enhancement.

values [95% CI]) between the observers in the evaluation of pathologies was good-to-excellent for ultrafast-DL-3DIIE and conventional images: 0.85 [0.81–0.89], 0.87 [0.85–0.89], 0.67 [0.61–0.73], 0.65 [0.60–0.70], 0.88 [0.85–0.91], 0.82 [0.78–0.86], respectively.

Table 5 exhibited the intra-protocol (conventional vs conventional) inter-observer and inter-protocol inter-observer agreement rates. It also showed the 95% CIs for the individual equivalence indices. For central canal stenosis, foraminal stenosis, endplate degeneration, disc herniation, and other pathologies, the highest upper bound of the 95% CI was within 5%, suggesting that the two protocols can be used interchangeably. However, the upper bound for disc degeneration was slightly higher at 5.45%.

Discussion

In summary, our study investigated both the image quality and diagnostic parity of our ultrafast cervical spine MRI protocols, which harnesses the DL-3DIIE system, against the traditional approach. Generally, the ultrafast-DL-3DIIE

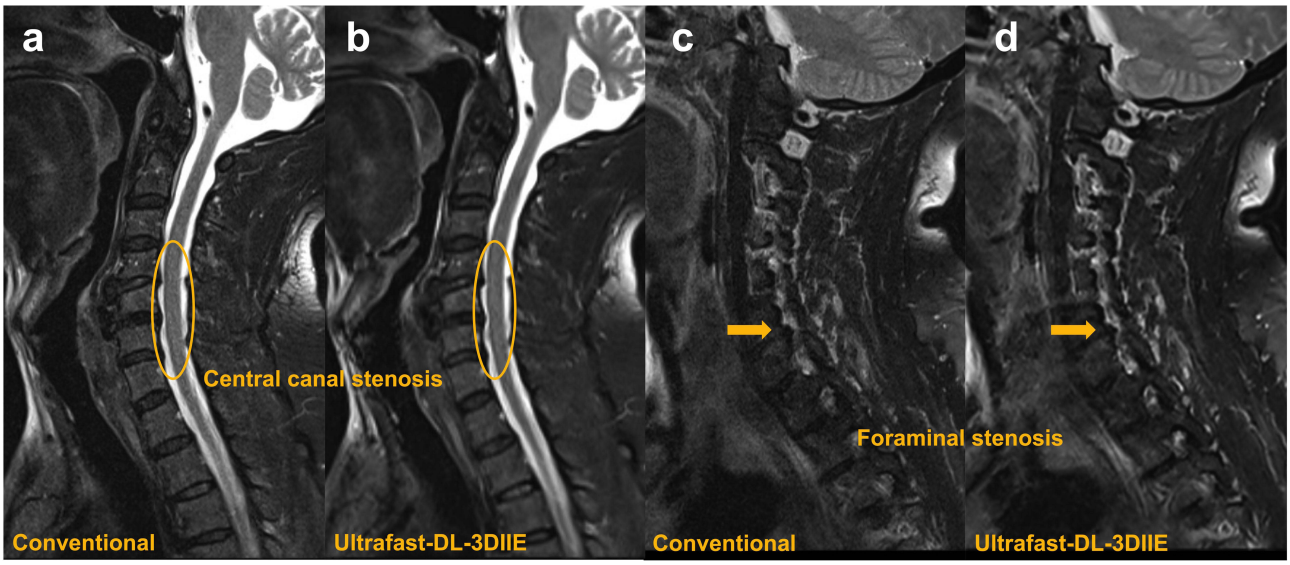

Figure 2 Sagittal T2-weighted images of a participant with central canal stenosis (C3-7 levels, Orange ellipses), were obtained from both conventional (**a**) and ultrafast-DL-3DIIE (**b**) protocols. And sagittal T2-weighted images of a participant with foraminal stenosis (C5-6 level, Orange arrows), obtained from both conventional (**c**) and ultrafast-DL-3DIIE (d) protocols.

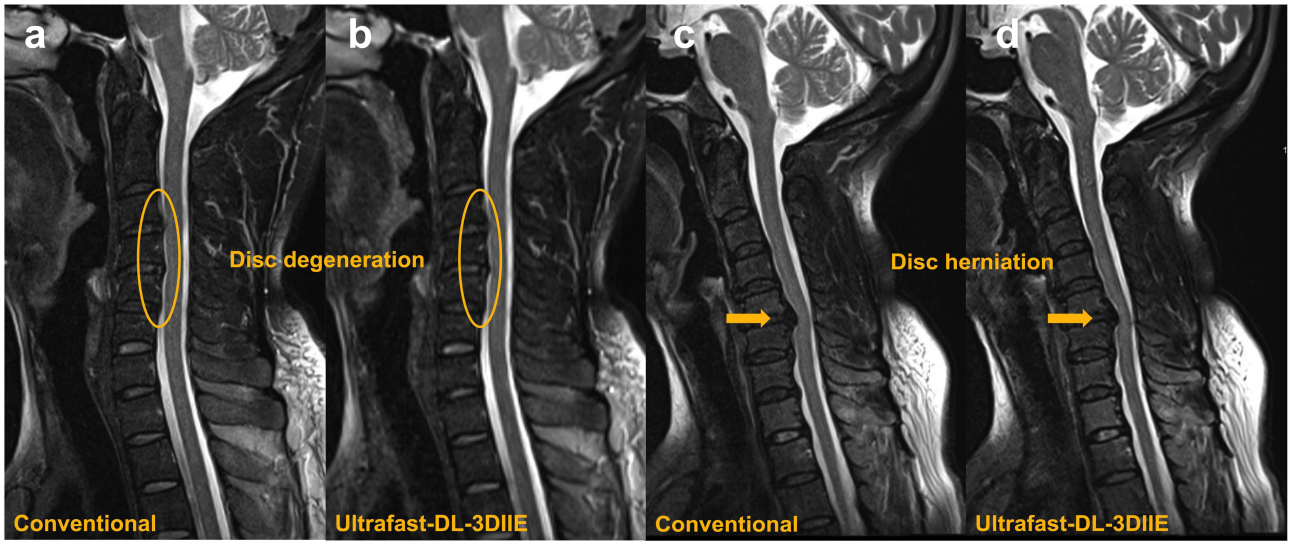

Figure 3 Sagittal T2-weighted images of a participant with disc degeneration (C3-4, C4-5 and C5-6 discs, Orange ellipses), were obtained from both conventional (**a**) and ultrafast-DL-3DIIE (**b**) protocols. And sagittal T2-weighted images of a participant with disc herniation (C5-6 disc, Orange arrows), obtained from both conventional (**c**) and ultrafast-DL-3DIIE (**d**) protocols.

images met the performance of conventional MRI. The prevalence of various pathologies detected was comparable between the ultrafast-DL-3DIIE and standard protocols. This equivalence was further reinforced by strong inter-protocol intra-observer concordance across all evaluated features. These findings suggest that our ultrafast cervical spine MRI protocol with deep learning-based image post-processing algorithm stands as a viable, time-efficient alternative for rapid scanning in routine physical examinations.

Our study demonstrates a strategy that achieves a substantial two-thirds reduction in scan time without utilizing raw data. Previously, ultrafast skeletal protocols based on DL reconstruction claimed to slash 77~85% scan time with diagnostic equivalence.[20,21] Our strategy reduces scan duration by 67% maintaining diagnostic ability with the help of the DL-3DIIE system. Please note, that despite the similar resolution, the conventional protocols in the previous studies[20,21] present a significantly longer duration than ours (187–193 vs 125 seconds per sequence). Also, the large reduced acquisition time has contributors of compressed sensing and enlarged slice thickness, which is controlled in our

Table 5 Interchangeability Results for Two Protocols

		Inter-Observer Agreement Rate	95% CI of the Individual Equivalence Index (%)
Central canal stenosis	Intra-protocol	52.9%	−2.93 to 1.13
	Inter-protocol	53.9%	
Foraminal stenosis	Intra-protocol	60.8%	−1.67 to 3.34
	Inter-protocol	58.8%	
Endplate degeneration	Intra-protocol	78.4%	−5.33 to 1.76
	Inter-protocol	79.4%	
Disc degeneration	Intra-protocol	92.1%	−2.11 to 5.45
	Inter-protocol	91.1%	
Disc herniation	Intra-protocol	76.5%	−2.42 to 4.41
	Inter-protocol	74.5%	
Other pathologies	Intra-protocol	82.4%	−3.51 to 4.78
	Inter-protocol	81.4%	

Note: Other pathologies included hyperintense cord lesion, retro-odontoid pseudotumor, spinal lipoma, vertebral fracture and vertebral hypointense lesion.
Abbreviation: CI, confidence interval.

study. In our strategy, the original ultrafast protocol maintains a high tissue SNR, providing a foundation for subsequent super-resolution and patch decomposition. This yields a crisp delineation of spinal components, including the spinal cord, CSF, vertebral bodies, and discs. Additionally, we noted an improved score in artifact reduction, likely due to reduced patient movement within the shortened scan durations. As expected, spine examination participants in our cohort were middle-aged or elderly people (average age 51.7±12.5), almost all suffering from musculoskeletal discomfort. The occurrence of motion artifacts does decrease compared to the routine 6-minute scan, as an expected advantage for such a strategy. Notably, the inferior score for the original ultrafast images might relate to increased Gibbs ringing from larger voxel sizes, which was effectively mitigated by the super-resolution.

Common pathology observed in spine MRI exams includes herniation, stenosis and degeneration. The former two are geometric changes while the last is contrast alteration. In this study, outpatients from a physical examination center turned out to be diagnosed with varied mild pathologies like central canal stenosis, foraminal stenosis, and disc issues. These conditions, often detectable by structural or contrast changes, are amenable to our acceleration approach. However, endplate degeneration seems to be an easily missed pathology for a single reader on the ultrafast protocol. Similar reports were found in the literature.[21] This might be explained by the magnified truncation artifacts parallel to the vertebral endplate in sagittal spine MRI due to fewer phase encoding steps. Minor anomalies, such as those at nerve rootlets requiring higher resolution, eluded our reduced-resolution protocol. Despite this, nerve rootlet assessment is not standard and is better served by higher-field MRI.[38] Comparatively, while the accelerated images slightly lose detail, the overall case detection rate aligns closely with the conventional protocol, underpinned by strong inter-protocol intra-observer concordance. To gain clinical endorsement, accelerated MRI must pass both participant and lesion-based tests for non-inferiority and uphold diagnostic accuracy. Leveraging a pathology grading system, Yasaka et al[39] reported deep learning's contribution to a notable rise in inter-observer consistency for spinal canal and neuroforaminal stenosis evaluation, even with fewer acquisitions. Kashiwagi et al[21] also confirmed the ultrafast protocol with DL reconstruction as a viable substitute for the traditional protocol, barring some nuances in endplate degeneration assessment. Our findings, alongside previous research, underscore the promise of DL in expediting standard spine MRI workflows without significant diagnostic trade-offs.

Our investigation offers new inspiration for ultrafast musculoskeletal MRI, by serially using conventional non-local means of denoising and DL super-resolution. Similar studies mainly concentrate on DL reconstruction[12–15,20,21] instead of DL post-processing, yet the latter holds inherent advantages of scanner-neutrality, flexibility, and capability for retrospective data leveraging. A workflow integrating post-processing techniques, both DL-based and conventional, is free to construct and optimize without any vendor or scanner restriction. In fact, the 3D iterative imaging enhancement applied in this study has been utilized in previous brain MRI and even CT studies without the DL module.[25,26] On the other hand, the advantage of discerning anatomical features through extensive training on large datasets is still reserved in DL post-processing techniques.[40] Such approaches are increasingly reported to show the ability to surpass traditional image enhancement approaches, which typically sacrifice structural clarity for noise reduction.[41] In this study, the 3DIIE algorithm contains patch-based self-similarity learning. This might be especially suitable for musculoskeletal MRI, where boundary delineation of components is of major clinical value. However, how effective could this approach be applied to other systems apart from the spine needs further validation.

We acknowledge the limitations of our research, particularly the small, specialized cohort and the use of a singular 1.5 T MRI scanner from one vendor, which may affect the broad-based application of our findings. Future research should broaden the scope with larger, varied cohorts and incorporate multi-vendor validation to fully ascertain the effectiveness and versatility of the ultrafast spine MRI protocol with the DL-3DIIE system. Furthermore, the implications of the DL-3DIIE system on diagnostic accuracy remain undefined, necessitating future comparative studies. These studies should aim to clarify the system's diagnostic impact across a wider array of spinal pathologies in a routine clinical setting.

Conclusion

Our investigation offers initial proof that the ultrafast cervical spine MRI protocol incorporating the DL-3DIIE system matches or surpasses the conventional protocol in qualitative, quantitative, and diagnostic outcomes. This supports the potential of the ultrafast approach for standard cervical spine MRI examinations.

Acknowledgments

The authors would like to express our enormous appreciation and gratitude to all participants.

Disclosure

The authors report no conflicts of interest in this work.

References

1. Ghaffari-Rafi A, Peterson C, Leon-Rojas JE, et al. The role of magnetic resonance imaging to inform clinical decision-making in acute spinal cord injury: a systematic review and meta-analysis. *J Clin Med*. 2021;10(21):4948. doi:10.3390/jcm10214948
2. Michelini G, Corridore A, Torlone S, et al. Dynamic MRI in the evaluation of the spine: state of the art. *Acta Biomed*. 2018;89(1–S):89.
3. Zaitsev M, Maclaren J, Herbst M. Motion artifacts in MRI: a complex problem with many partial solutions. *J Magn Reson Imaging*. 2015;42(4):887–901. doi:10.1002/jmri.24850
4. Gao T, Lu Z, Wang F, Zhao H, Wang J, Pan S. Using the compressed sensing technique for lumbar vertebrae imaging: comparison with conventional parallel imaging. *Curr Med Imaging*. 2021;17(8):1010–1017. doi:10.2174/1573405617666210126155814
5. Longo MG, Fagundes J, Huang S, et al. Simultaneous multislice-based 5-minute lumbar spine MRI protocol: initial experience in a clinical setting. *J Neuroimaging*. 2017;27(5):442–446. doi:10.1111/jon.12453
6. Nolte I, Gerigk L, Brockmann MA, Kemmling A, Groden C. MRI of degenerative lumbar spine disease: comparison of non-accelerated and parallel imaging. *Neuroradiology*. 2008;50(5):403–409. doi:10.1007/s00234-008-0363-0
7. Qiu J, Liu J, Bi Z, et al. An investigation of 2D spine Magnetic Resonance Imaging (MRI) with Compressed Sensing (CS). *Skeletal Radiol*. 2022;51(6):1273–1283. doi:10.1007/s00256-021-03954-x
8. Glockner JF, Hu HH, Stanley DW, Angelos L, King K. Parallel MR imaging: a user's guide. *Radiographics*. 2005;25(5):1279–1297. doi:10.1148/rg.255045202
9. Stenger VA, Noll DC, Boada FE. Partial Fourier reconstruction for three-dimensional gradient echo functional MRI: comparison of phase correction methods. *Magn Reson Med*. 1998;40(3):481–490. doi:10.1002/mrm.1910400320
10. Jaspan ON, Fleysher R, Lipton ML. Compressed sensing MRI: a review of the clinical literature. *Br J Radiol*. 2015;88(1056):20150487. doi:10.1259/bjr.20150487
11. Johnson PM, Recht MP, Knoll F. Improving the Speed of MRI with Artificial Intelligence. *Semin Musculoskelet Radiol*. 2020;24(1):12–20. doi:10.1055/s-0039-3400265
12. Kashiwagi N, Tanaka H, Yamashita Y, et al. Applicability of deep learning-based reconstruction trained by brain and knee 3T MRI to lumbar 1.5T MRI. *Acta Radiol Open*. 2021;10(6):20584601211023939. doi:10.1177/20584601211023939
13. Xie Y, Tao H, Li X, et al. Prospective comparison of standard and deep learning-reconstructed turbo spin-echo MRI of the shoulder. *Radiology*. 2024;310(1):e231405. doi:10.1148/radiol.231405
14. Herrmann J, Gassenmaier S, Nickel D, et al. Diagnostic confidence and feasibility of a deep learning accelerated HASTE sequence of the abdomen in a single breath-hold. *Invest Radiol*. 2021;56(5):313–319. doi:10.1097/RLI.0000000000000743
15. Ogawa R, Kido T, Nakamura M, et al. Reconstruction of cardiovascular black-blood T2-weighted image by deep learning algorithm: a comparison with intensity filter. *Acta Radiologica Open*. 2021;10(9):205846012110447. doi:10.1177/20584601211044779
16. Zhao ST, Cahill DG, Li SY, et al. Denoising of three-dimensional fast spin echo magnetic resonance images of knee joints using spatial-variant noise-relevant residual learning of convolution neural network. *Comput Biol Med*. 2022;151:106295.
17. Kumar MG, Das Goswami A. Automatic classification of the severity of knee osteoarthritis using enhanced image sharpening and CNN. *Appl Sci-Basel*. 2023;13(3):1658.
18. Chaudhari AS, Fang ZN, Kogan F, et al. Super-resolution musculoskeletal MRI using deep learning. *Magnet Reson Med*. 2018;80(5):2139–2154. doi:10.1002/mrm.27178
19. Yoon MA, Gold GE, Chaudhari AS. Accelerated musculoskeletal magnetic resonance imaging. *J Magn Reson Imaging*. 2023. doi:10.1002/jmri.29205
20. Fujiwara M, Kashiwagi N, Matsuo C, et al. Ultrafast lumbar spine MRI protocol using deep learning-based reconstruction: diagnostic equivalence to a conventional protocol. *Skeletal Radiol*. 2023;52(2):233–241. doi:10.1007/s00256-022-04192-5
21. Kashiwagi N, Sakai M, Tsukabe A, et al. Ultrafast cervcial spine MRI protocol using deep learning-based reconstruction: diagnostic equivalence to a conventional protocol. *Eur J Radiol*. 2022;156:110531. doi:10.1016/j.ejrad.2022.110531
22. Coupé P, Yger P, Prima S, Hellier P, Kervrann C, Barillot C. An optimized blockwise nonlocal means denoising filter for 3-D magnetic resonance images. *IEEE Transac Med Imaging*. 2008;27(4):425–441. doi:10.1109/TMI.2007.906087
23. Bustin A, Voilliot D, Menini A, et al. Isotropic reconstruction of MR images using 3D patch-based self-similarity learning. *IEEE Transac Med Imaging*. 2018;37(8):1932–1942. doi:10.1109/TMI.2018.2807451
24. Manjón JV, Coupé P, Buades A, Fonov V, Collins DL, Robles M. Non-local MRI upsampling. *Med Image Anal*. 2010;14(6):784–792. doi:10.1016/j.media.2010.05.010
25. Padole A, Singh S, Ackman JB, et al. Submillisievert chest CT with filtered back projection and iterative reconstruction techniques. *AJR Am J Roentgenol*. 2014;203(4):772–781. doi:10.2214/AJR.13.12312
26. Kanemaru N, Takao H, Amemiya S, Abe O. The effect of a post-scan processing denoising system on image quality and morphometric analysis. *J Neuroradiol*. 2022;49(2):205–212. doi:10.1016/j.neurad.2021.11.007
27. Buades A, Coll B, Morel JM. A non-local algorithm for image denoising. Conference on Computer Vision and Pattern Recognition; San Diego, CA; 2005:60–65.
28. Fardon DF, Williams AL, Dohring EJ, Murtagh FR, Gabriel Rothman SL, Sze GK. Lumbar disc nomenclature: version 2.0: recommendations of the combined task forces of the North American Spine Society, the American Society of Spine Radiology and the American Society of Neuroradiology. *Spine J*. 2014;14(11):2525–2545. doi:10.1016/j.spinee.2014.04.022

29. Fu MC, Webb ML, Buerba RA, et al. Comparison of agreement of cervical spine degenerative pathology findings in magnetic resonance imaging studies. *Spine J*. 2016;16(1):42–48. doi:10.1016/j.spinee.2015.08.026
30. Kang Y, Lee JW, Koh YH, et al. New MRI grading system for the cervical canal stenosis. *AJR Am J Roentgenol*. 2011;197(1):W134–W140. doi:10.2214/AJR.10.5560
31. Kim SJ, Lee TH, Yi S. Prevalence of disc degeneration in asymptomatic Korean subjects. Part 3: cervical and lumbar relationship. *J Korean Neurosurg Soc*. 2013;53(3):167–173. doi:10.3340/jkns.2013.53.3.167
32. Lee KH, Park HJ, Lee SY, et al. Inter-observer reliability and clinical validity of the MRI grading system for cervical central stenosis based on sagittal T2-weighted image. *Eur J Radiol*. 2020;127:108987. doi:10.1016/j.ejrad.2020.108987
33. Lee S, Lee JW, Yeom JS, et al. A practical MRI grading system for lumbar foraminal stenosis. *AJR Am J Roentgenol*. 2010;194(4):1095–1098. doi:10.2214/AJR.09.2772
34. Miyazaki M, Hong SW, Yoon SH, Morishita Y, Wang JC. Reliability of a magnetic resonance imaging-based grading system for cervical intervertebral disc degeneration. *J Spinal Disord Tech*. 2008;21(4):288–292. doi:10.1097/BSD.0b013e31813c0e59
35. Modic MT, Ross JS. Lumbar degenerative disk disease. *Radiology*. 2007;245(1):43–61. doi:10.1148/radiol.2451051706
36. Obuchowski NA, Subhas N, Schoenhagen P. Testing for interchangeability of imaging tests. *Acad Radiol*. 2014;21(11):1483–1489. doi:10.1016/j.acra.2014.07.004
37. Zanchi F, Richard R, Hussami M, Monier A, Knebel JF, Omoumi P. MRI of non-specific low back pain and/or lumbar radiculopathy: do we need T1 when using a sagittal T2-weighted Dixon sequence? *Eur Radiol*. 2020;30(5):2583–2593. doi:10.1007/s00330-019-06626-6
38. Galley J, Sutter R, Germann C, Wanivenhaus F, Nanz D. High-resolution in vivo MR imaging of intraspinal cervical nerve rootlets at 3 and 7 Tesla. *Eur Radiol*. 2021;31(7):4625–4633. doi:10.1007/s00330-020-07557-3
39. Yasaka K, Tanishima T, Ohtake Y, et al. Deep learning reconstruction for 1.5 T cervical spine MRI: effect on interobserver agreement in the evaluation of degenerative changes. *Eur Radiol*. 2022;32(9):6118–6125. doi:10.1007/s00330-022-08729-z
40. Uetani H, Nakaura T, Kitajima M, et al. A preliminary study of deep learning-based reconstruction specialized for denoising in high-frequency domain: usefulness in high-resolution three-dimensional magnetic resonance cisternography of the cerebellopontine angle. *Neuroradiology*. 2021;63(1):63–71. doi:10.1007/s00234-020-02513-w
41. Mishro PK, Agrawal S, Panda R, Abraham A. A survey on State-of-the-Art Denoising techniques for brain magnetic resonance images. *IEEE Rev Biomed Eng*. 2022;15:184–199. doi:10.1109/RBME.2021.3055556